AMERICAN SOCIETY FOR MICROBIOLOGY | Journal of Virology®

In Vitro Replication of Chelonid Herpesvirus 5 in Organotypic Skin Cultures from Hawaiian Green Turtles (*Chelonia mydas*)

Thierry M. Work,[a] Julie Dagenais,[a] Tina M. Weatherby,[b] George H. Balazs,[c] Mathias Ackermann[d]

U.S. Geological Survey, National Wildlife Health Center, Honolulu Field Station, Honolulu, Hawaii, USA[a]; Biological EM Facility, University of Hawaii, Honolulu, Hawaii, USA[b]; NOAA, National Marine Fisheries Service, Pacific Islands Fisheries Science Center, Honolulu, Hawaii, USA[c]; Institute of Virology, University of Zurich, Zurich, Switzerland[d]

ABSTRACT Fibropapillomatosis (FP) is a tumor disease of marine turtles associated with chelonid herpesvirus 5 (ChHV5), which has historically been refractory to growth in tissue culture. Here we show, for the first time, *de novo* formation of ChHV5-positive intranuclear inclusions in cultured green turtle cells, which is indicative of active lytic replication of the virus. The minimal requirements to achieve lytic replication in cultured cells included (i) either *in vitro* cultures of ChHV5-positive tumor biopsy specimens (plugs) or organotypic cultures (rafts) consisting of ChHV5-positive turtle fibroblasts in collagen rafts seeded with turtle keratinocytes and (ii) keratinocyte maturation induced by raising raft or biopsy cultures to the air-liquid interface. Virus growth was confirmed by detailed electron microscopic studies that revealed intranuclear sun-shaped capsid factories, tubules, various stages of capsid formation, nuclear export by budding into the perinuclear space, tegument formation, and envelopment to complete *de novo* virus production. Membrane synthesis was also observed as a sign of active viral replication. Interestingly, cytoplasmic particles became associated with keratin filaments, a feature not seen in conventional monolayer cell cultures, in which most studies of herpesvirus replication have been performed. Our findings draw a rich and realistic picture of ChHV5 replication in cells derived from its natural host and may be crucial not only to better understand ChHV5 circulation but also to eventually complete Koch's postulates for FP. Moreover, the principles described here may serve as a model for culture of other viruses that are resistant to replication in conventional cell culture.

IMPORTANCE A major challenge in virology is the study of viruses that cannot be grown in the laboratory. One example is chelonid herpesvirus 5 (ChHV5), which is associated with fibropapillomatosis, a globally distributed, debilitating, and fatal tumor disease of endangered marine turtles. Pathological examination shows that ChHV5 is shed in skin. Here we show that ChHV5 will grow *in vitro* if we replicate the complex three-dimensional structure of turtle skin. Moreover, lytic virus growth requires a close interplay between fibroblasts and keratinocytes. Finally, the morphogenesis of herpesviral growth in three-dimensional cultures reveals a far richer, and likely more realistic, array of capsid morphologies than that encountered in traditional monolayer cell cultures. Our findings have applications to other viruses, including those of humans.

KEYWORDS herpesvirus, electron microscopy, immunohistochemistry, morphogenesis, pathobiology

Received 10 March 2017 **Accepted** 2 June 2017

Accepted manuscript posted online 14 June 2017

Citation Work TM, Dagenais J, Weatherby TM, Balazs GH, Ackermann M. 2017. *In vitro* replication of chelonid herpesvirus 5 in organotypic skin cultures from Hawaiian green turtles (*Chelonia mydas*). J Virol 91:e00404-17. https://doi.org/10.1128/JVI.00404-17.

Editor Klaus Frueh, Oregon Health & Science University

Address correspondence to Thierry M. Work, Thierry_work@usgs.gov.

Seven species of sea turtles exist globally, the most common of which is the green turtle (*Chelonia mydas*) (1). Green turtles are listed as threatened or endangered throughout their range by the U.S. Endangered Species Act and the International Union for the Conservation of Nature (IUCN; except in Hawaii, where they are listed as near threatened by the IUCN); threats include loss of nesting habitat, nest depredation, and bycatch in commercial fisheries (2). Diseases have also been documented for green turtles; the most common of these is fibropapillomatosis (FP), a disease that has a global distribution (3) and causes disfiguring tumors on the skin, eyes, and mouth as well as internal tumors, mostly in the lungs, heart, and kidneys (4, 5). FP has been seen in most places where green turtles range and has been studied most extensively in Hawaii, Florida, Brazil, and Australia (3, 6). Severely affected turtles become immunosuppressed, septic, and emaciated and eventually die (7, 8). In Hawaii, FP continues to be a leading cause of debilitation and stranding of green turtles, although the disease there is waning, for unknown reasons (9). In contrast, in Florida (10) and Brazil (11), the prevalence of FP remains relatively constant.

FP is likely caused by an infectious agent. Experimentally, FP is transmissible in green turtles by use of cell-free filtrates (12), and the disease appears to be contagious in captive turtles (13). Although numerous etiologies and cofactors have been proposed for FP, including parasites (14), marine toxins (15), pollutants (16), and habitat eutrophication (17), the most likely cause is a herpesvirus. On light microscopy, epidermal intranuclear inclusions (EII) have been seen in tumors that on electron microscopy contain herpesvirus-like particles (18). Additionally, herpesviral DNA is consistently detected in tumor tissues, but less commonly in nontumor tissues, from turtles from Hawaii (19), Florida (20), and Brazil (21). In 2012, the virus associated with FP, chelonid herpesvirus 5 (ChHV5), was designated the type for the newly erected genus *Scutavirus* of the subfamily *Alphaherpesvirinae*, family *Herpesviridae* (22).

A big limitation to our understanding of the pathogenesis and epidemiology of FP in green turtles is the inability to grow ChHV5 *in vitro*. In nature, lytic viral production infrequently occurs in keratinocytes (KC) of skin tumors (23). Extensive attempts to grow the virus by using cultured normal or tumor fibroblasts (FB) or KC monolayers from green turtles in the presence or absence of compounds that induce herpesvirus growth *in vitro* have failed. Apparently, the virus persists in a predominantly latent state, and infectivity is lost as cells are passaged (24). In this context, ChHV5 resembles certain other herpesviruses, such as human herpesvirus 8, that are difficult to culture *in vitro* (25) and that contrast with more easily cultured herpesviruses, such as herpes simplex virus (HSV) (26). The inability to culture ChHV5 has stymied attempts to fulfill Koch's postulates and to develop serological tests, thereby limiting our understanding of the epidemiology of FP or potential routes of transmission.

ChHV5 appears to be more akin to papillomaviruses (27) in requiring stratified KC to undergo lytic replication. As such, organotypic cultures might provide an alternate means of culturing ChHV5 by recapitulating the three-dimensional (3D) structure of turtle skin, including the dermis, basement membrane, and strata basale, spinosum, granulosum, and corneum (28). Organotypic cultures were first developed in the late 1970s by Green and colleagues, who constructed rafts of collagen embedded with mouse FB and overlaid with cultured KC that were raised to the air-liquid interface, thereby stimulating stratification of KC from the stratum basale to the stratum corneum (29). This system then allowed *in vitro* cultivation of papillomaviruses that heretofore had been refractory to cell culture (27).

The present study provides new insights into herpesviral replication. Here we show that ChHV5 will grow in green turtle skin biopsy specimens (plugs) and organotypic cultures (rafts). Our findings are the first instance of using this method for a nonmammalian organism and of culturing ChHV5 *in vitro*. Although rafts have been developed for other mammals, such as rats (30), dogs (31), and horses (32), we know of no such system for members of the Reptilia (birds and reptiles). The ability to maintain tumor explants *in vitro* may be a tool for understanding broader questions in tumor cell biology, wound repair, and epitheliotropic herpesviral reproduction in reptiles.

RESULTS

Origin of tissues. We obtained plugs from 90 tumors and 10 sections of normal skin (neck) from 24 turtles, sampling 1 to 7 (mean = 4) tumors/case. Tumors originated mostly from the front flippers (51%), neck (19%), rear flippers (14%), jaw hinge (10%), cloaca (1%), eye (1%), glottis (1%), and unrecorded locations (remainder). Of the 90 tumors sampled, we performed histological examinations on 52, and EII were detected in 9 (17%) tumors. Forty-five of the 52 tumors assessed histologically were measured and had surface areas ranging from 3 to 10,600 cm^2 (mean ± standard deviation [SD] = 297 ± 1,228 cm^2). There was no significant relationship between tumor size and the presence of EII ($P = 0.0491$); however, the statistical power to detect this by logistic regression given our sample size and the variability of the tumor measurements was low.

Light microscopy analysis of cultured plugs. We examined 1,073 cultured plugs by histology; 176 originated from normal skin, and the remainder originated from tumors. Of 176 cultured plugs from normal skin, 139 had an intact epidermis, and none had EII. Of 892 cultured plugs from tumors, 753 had an intact epidermis, and of these, 87 (11.5%) had locally extensive ballooning degeneration of the epidermis, with EII exclusively in the epidermis (Fig. 1a and b). In areas of ballooning degeneration, green turtles mounted an immune response to EII and cell membranes, as measured by reactivity of anti-turtle IgY monoclonal antibodies (MAbs) to turtle 7S IgY (Fig. 1c), whereas an anti-ChHV5 VP26 rat polyclonal antibody decorated mainly nuclei and cell membranes faintly (Fig. 1d). Negative controls (FP-positive serum against normal skin, FP-negative serum against inclusions, and FP-positive serum with a *Campylobacter* MAb) failed to decorate inclusions.

Of the 753 cultured plugs with intact epidermis, 693 came from tumors with measurements, and these were used to statistically analyze culture conditions conducive to formation of EII. Of the factors analyzed (tumor size, number of days that plugs were equilibrated submerged, number of days that plugs were cultured at the air-liquid interface, and use of inducers), none contributed significantly to formation of EII (Table 1). To assess whether tumor culture influenced EII production, we examined the histology of separate samples of 52 tumors prior to and after culture. While only 17% (9 of 52 tumors) of tumors had EII, the detection rate for EII in tissues from the same tumors after culture increased to 42% (22 of 52 tumors), a difference that was statistically significant ($\chi^2 = 7.8$; $P = 0.0095$; odds ratio [OR] = 3.5 [95% confidence interval {CI} = 1.4 to 8.1]), thereby confirming that tissue culture increased virus production. Of 33 tumors from which EII-positive plugs were cultured, 21 originated from front flippers, 6 from the neck, 2 each from the rear flipper and mouth, and 1 each from the cloaca and eye.

Light microscopy analysis of rafts. For rafts, FB originated from 27 turtles (21 tumors and 11 normal skins), whereas KC originated from 13 turtles (14 tumors and 8 normal skins). Of 87 rafts attempted, 69 developed an intact stratified epidermis with a stratum corneum, and of these, 8 (11%) presented ballooning degeneration and EII exclusively in the epidermis (Fig. 1e and f). Compared to the result for plugs, there was more uniform reactivity to 7S IgY for FP-positive turtles (Fig. 1g), whereas the anti-VP26 polyclonal antibody reacted mainly with nuclei (Fig. 1h). Negative-control tissues failed to show reactivity to inclusions. When the tumor status (positive [+] or negative [−]) of FB or KC was examined for an influence on formation of EII in rafts, the following four combinations were possible: FB^+ KC^+, FB^+ KC^-, FB^- KC^+, and FB^- KC^-. Proportions of attempts for each of these categories yielding EII in rafts were as follows: FB^+ KC^+, 7/30 attempts (23%); FB^+ KC^-, 1/19 attempts (5%); FB^- KC^+, 0/14 attempts (0%); and FB^- KC^-, 0/16 attempts (0%). Interestingly, EII were seen only in rafts created using early-passage tumor fibroblasts known to be positive for viral DNA (24). It appeared that tumor KC were more permissive to lytic viral growth and formation of EII than nontumor KC, although neither contained viral DNA in the absence of tumor FB (24). Moreover, of the culture parameters analyzed by logistic regression, only the number

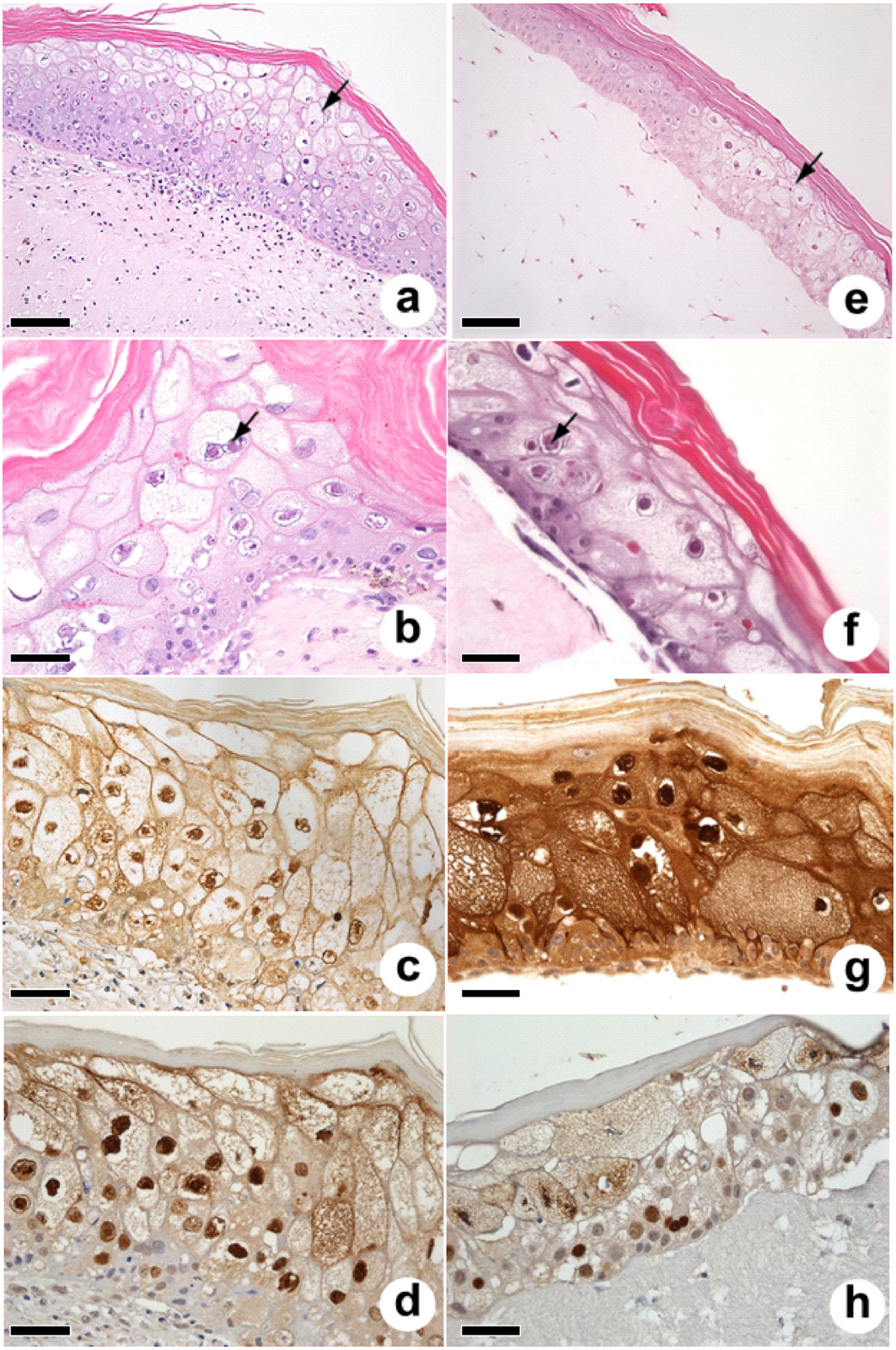

FIG 1 Light microscopy of plugs (a to d) and rafts (e to h). Note the stratified epidermis (a and e) with ballooning degeneration (arrows) and the somewhat less cellular collagen matrix for the raft (e) than the denser, more cellular dermis with the plug (a). Note the presence of EII (arrows) in the epidermis in plugs (b) and rafts (f). Turtle 7S IgY reactivity as assayed by monoclonal antibodies recognizes EII and cell membranes in plugs (c), whereas staining of the raft epidermis is more intense (g). In contrast, the anti-VP26 polyclonal antibody recognizes mainly nuclei in plugs (d) and rafts (h). Culture conditions were as follows. (a to d) Plugs incubated submerged for 4 days and at the air-liquid interface for 17 days. (e and h) Raft tumor FB gels

(Continued on next page)

TABLE 1 Contributions of tissue culture conditions to formation or maintenance of epidermal intranuclear inclusions in plugs[a]

Parameter	Log odds	95% CI		χ^2 value	*P* value
		Lower	Upper		
Tumor surface area	0	−0.001	0	0.354	0.552
Time (days) that plug was submerged	0.106	−0.123	0.337	0.816	0.366
Time (days) that plug was at air-liquid interface	0.052	−0.011	0.119	2.583	0.108
No inducer	−0.088	−2.361	4.807	0.003	0.954
Sodium butyrate	1.039	−1.475	5.992	0.531	0.466
Dexamethasone	0.583	−4.784	5.959	0.073	0.787
Epinephrine	0.499	−4.94	5.96	0.05	0.823
Forskolin	−1.049	−4.225	4.028	0.31	0.578
Hexamethylenebisacetamide	−0.005	−5.332	5.322	0	0.998
Iododeoxyuridine	−0.991	−6.313	4.328	0.216	0.642
Tumor necrosis factor	−0.51	−5.817	4.793	0.059	0.808
Phorbol 12-myristate 13-acetate	1.24	−1.059	6.141	0.91	0.34
Trichostatin A	−0.289	−5.679	5.111	0.018	0.894

[a]The data are the results of analysis by Firth's logistic regression. No data are given for valproic acid or 5-azacytidine because rafts for these plugs did not have an intact epidermis to examine by histology.

of days that collagen rafts were incubated prior to addition of KC contributed significantly to the formation of EII, and the α value was marginally lower than 0.05 (Table 2). These observations clearly emphasize the need for cell culture and the requirement for the organotypic arrangement, with intimate contact between tumor FB and KC, which greatly enhanced the generation of EII.

Electron microscopy analysis of nuclear morphology. Electron microscopy of normal turtle skin revealed the basement membrane and the strata basale (Fig. 2a), spinosum, granulosum, and corneum, with no ballooning degeneration or virus-associated structures in the cytoplasm or nucleus. Compared to healthy cells from nontumor skin, cells from plug cultures had histologic evidence of ballooning degeneration (Fig. 2b), with a markedly vacuolated cytoplasm and enlarged swollen nuclei with marginated chromatin and ill-defined nuclear membranes. Within the nucleus, aggregates of capsids were sometimes seen within or around dense or reticulated nuclear bodies. Dense bodies were round, ranged from 927 to 2,671 nm (mean $\pm$ SD, 1,706 $\pm$ 508 [$n = 15$]) in diameter (Fig. 2c), and were surrounded by a unilayer corona of capsids (Fig. 2d), looking similar to intranuclear sun-like structures described previously in the herpesvirus literature (33–37). Tangential sections of these bodies suggested that they were uniformly covered with or consisted of capsids (Fig. 2e). Reticulated bodies were more amorphous, ranged from 786 to 1,823 nm (1,128 $\pm$ 420 [$n = 6$]) at their widest point, and had variably sized irregular internal cavities populated by capsids, some of which looked to be in the process of being assembled (Fig. 2f and 3a). Occasional tubular arrays of crystalline material were seen in the nucleus, associated with capsids. These tubules, with an outer diameter of ca. 80 nm, appeared to segment and constrict at the ends, eventually forming spheres (Fig. 3b and c). Apparent reduplication of nuclear membranes was evident (Fig. 3d). Virus-infected nuclei from plugs contained five distinct morphologies of viral capsids. Stippled scaffold capsids (Fig. 4a and 5a) were oblong with irregularly arranged internal dots, clear capsids (Fig. 4b and 5a) had no internal structures, targetoid scaffold capsids (Fig. 4c and 5a) were clear with a round or linear central electron-dense core, concentric capsids (Fig. 2f and 4d) enclosed a circular scaffold, and solid capsids (Fig. 4f and 5b) had a

FIG 1 Legend (Continued)
were incubated submerged for 7 days, and tumor KC were then added and incubated submerged for 6 days and at the air-liquid interface for 11 days. (f) Raft tumor FB gel was incubated submerged for 1 day, and tumor KC were then added and incubated submerged for 2 days and at the air-liquid interface for 13 days. (g) Raft tumor FB gel seeded with tumor KC and cultured submerged for 7 days and at the air-liquid interface for 13 days. Bars = 100 μm for panels a and e and 50 μm for all other panels.

TABLE 2 Contributions of tissue culture parameters to formation of epidermal intranuclear inclusions in rafts[a]

Parameter	Log odds	95% CI		χ^2 value	*P* value
		Lower	Upper		
Keratinocyte (KC) passage no.	0.21200	−0.14100	0.58000	1.46725	0.22578
Collagen concn (mg/ml)	−0.69300	−3.24000	0.58200	1.06324	0.30248
No. of fibroblasts/ml of collagen	0.00000	−0.00001	0.00001	0.00257	0.95955
Time (h) the collagen raft was allowed to shrink	0.02860	−0.01560	0.07730	1.72554	0.18898
Day that collagen raft detached from well	−0.02380	−0.33500	0.34700	0.02203	0.88201
Shrinking temp of collagen raft	0.05020	−0.90500	0.59400	0.02569	0.87265
Time (days) that collagen raft was incubated prior to addition of KC	0.84000	0.03290	1.95000	4.18706	0.04073
KC/surface area of raft	−0.00005	−0.00021	0.00002	1.94728	0.16288
Time (days) that raft was submerged	0.48600	−0.03890	1.27000	3.32585	0.06820
Time (days) that raft was at air-liquid interface	0.13800	−0.25500	0.80200	0.50773	0.47612

[a]The data are the results of analysis by Firth's logistic regression.

uniform electron-dense appearance. Of 971 capsids enumerated for 19 nuclei, 734 (75.6%) were stippled, followed by 123 (12.7%) clear, 95 (9.8%) concentric, 16 (1.6%) targetoid, and 3 (0.3%) solid capsids. There was no significant difference in diameter for all five capsid types (Table 3). Of 44 plug cells examined by electron microscopy, 7 (16%) had dense bodies, 8 (18%) had reticulated bodies, 9 (20%) had crystalline arrays, and 6 (14%) had apparent reduplication of the nuclear membrane.

The cell pathology of rafts was broadly similar to that of plugs. Of 647 nuclear capsids enumerated for 18 nuclei, 529 (82%) were concentric (Fig. 5c), 91 (14%) were clear, 17 (3%) were solid, and the remainder were targetoid; stippled capsids were absent. Reticulated bodies with partially formed capsids and tubules were present (Fig. 5d), round dense bodies were absent, and capsids within the cytoplasm were rare. Capsids within the nucleus were about the same size in rafts as those in plugs (Table 3). Of 20 cells enumerated for rafts, 4 had reticulated bodies and 6 had tubules within the nucleus.

Electron microscopy analysis of cytoplasmic morphology. Capsids were rarely seen transiting between the nucleus and the cytoplasm by budding (Fig. 5e), whereupon they appeared to accumulate near the nucleus and become associated with keratin filaments (Fig. 5f). Within the cytoplasm of cells from plugs, three types of round to elliptical viral particles were seen, including nontegumented and tegumented types (Fig. 6a) and enveloped particles encompassing single (Fig. 6b) and multiple (Fig. 6c) capsids. Nontegumented and tegumented capsids were associated with electron-dense keratin filaments, whereas enveloped capsids were more often associated with vesicles and delicate fibrils. Electron-dense material with capsids appeared to be sequestered at edges of affected cells (Fig. 6d). Of 1,003 particles enumerated from the cytoplasm of 51 cells from plugs, tegumented particles were most common (587 particles [58.5%]), followed by nontegumented particles (301 particles [30%]), with enveloped particles comprising the remainder. Cytoplasmic capsids were twice as large as those in the nucleus, and there was no significant difference in mean diameter between capsid morphologies within the cytoplasm (Table 3). Within rafts, cytoplasmic capsids were encountered infrequently but were similar to those in plugs.

DISCUSSION

Growth of ChHV5 requires intimate contact between fibroblasts and keratinocytes. The presence of a herpesvirus associated with FP has been known for over 20 years (18), yet the virus has been refractory to *in vitro* culture (24). This is the first time that organotypic skin or plug cultures have been developed for a nonmammalian host, allowing lytic growth of ChHV5 as confirmed by immunohistochemistry and electron microscopy. Two lines of evidence suggest that we actually replicated the virus *de novo* rather than merely maintaining existing virus in culture. First, for plugs, the >3-fold increase in the odds of obtaining EII in tissues from tumors after culture argues strongly that we were generating EII *in vitro*. Second, for rafts, the presence of stratified KC with

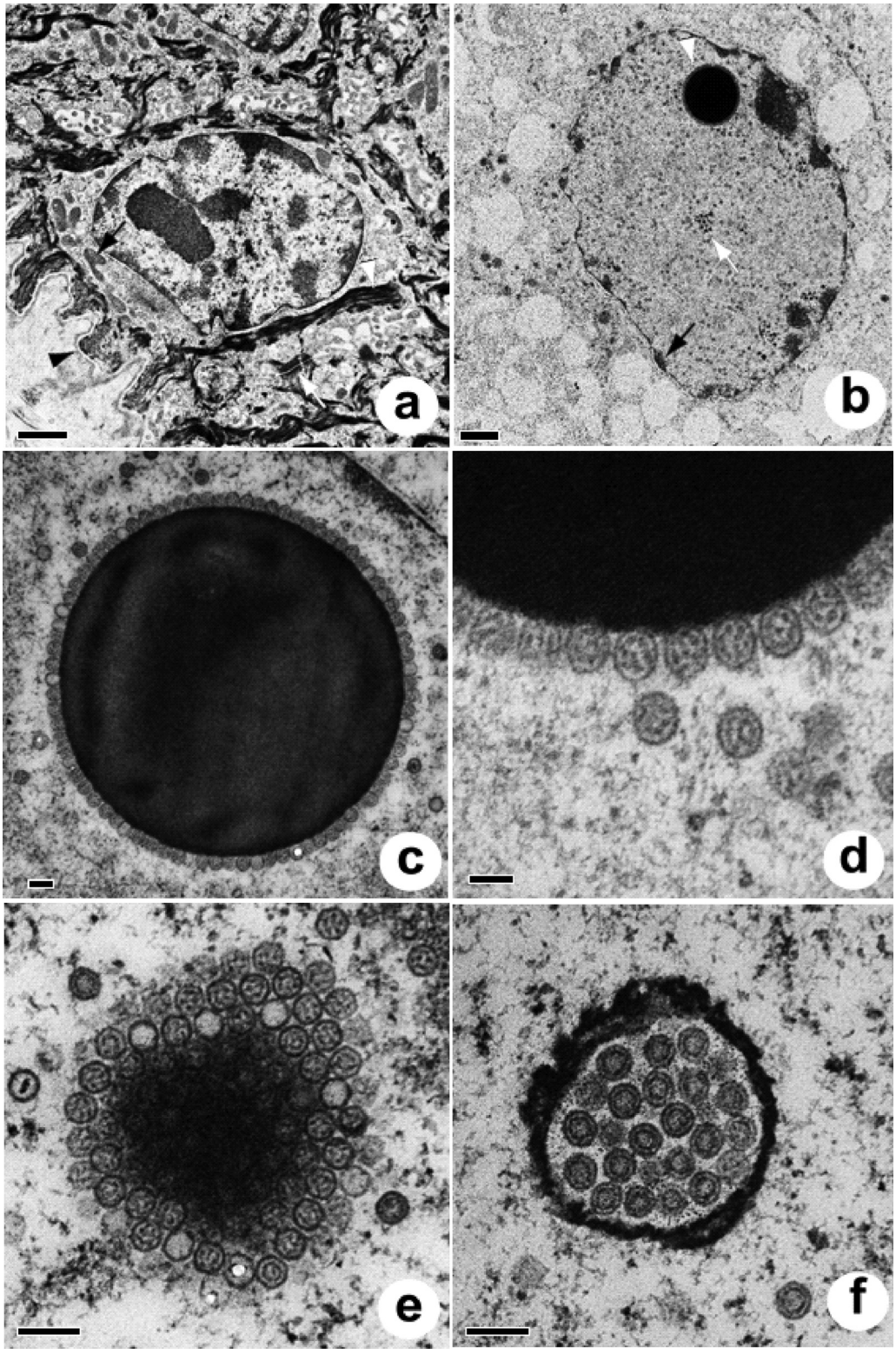

FIG 2 Electron micrographs of normal skin and plug nuclei. (a) Healthy keratinocyte (stratum basale) from normal skin. Note the basement membrane (black arrowhead), mitochondria (black arrow), keratin filaments (white arrowhead), and indistinct cell borders delineated by desmosomes (white arrow). Bar = 1 μm. (b) Keratinocyte infected with ChHV5. Note the enlarged swollen nucleus with marginated chromatin (black arrow), numerous capsids (white arrow), and the round dense body surrounded by capsids (white arrowhead), all of which are surrounded by markedly vacuolated cytoplasm. Bar = 1 μm. (c) Dense intranuclear body surrounded by a uniform array of stippled capsids. Bar = 200 nm. (d) Detail of dense intranuclear body. Bar = 100 nm. (e) Tangential section through a dense intranuclear body. Note the capsids in various planes of the section. Bar = 200 nm. (f) Reticulated intranuclear body replete with concentric capsids. Bar = 200 nm.

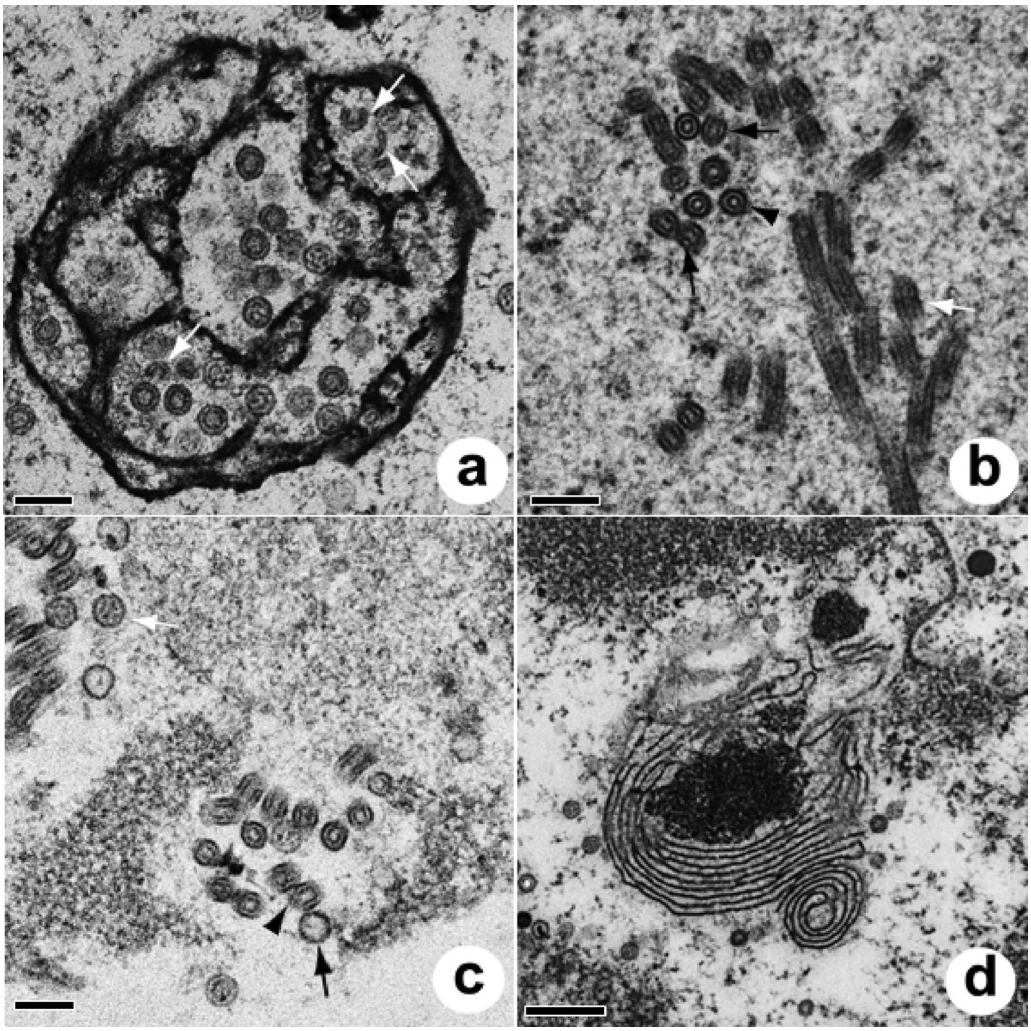

FIG 3 Electron micrographs of plug nuclei (continued). (a) Reticulated intranuclear body containing concentric or stippled capsids. Note the presence of partially formed capsids (white arrows). Bar = 200 nm. (b) Intranuclear crystalline tubular arrays. Note the segmentation of tubules (white arrow) apparently progressing to constriction of the ends of the segment (black arrow) and to a circular form (arrowhead). Bar = 200 nm. (c) Intranuclear crystalline arrays. Note the clear (black arrow) and stippled (white arrow) capsids nearby and tubular fragments apparently in the process of constricting at the ends (arrowhead). Bar = 200 nm. (d) Apparent reduplication of nuclear membranes. Bar = 500 nm.

ballooning degeneration and EII further supported the hypothesis that viral replication was occurring *de novo*, because turtle KC in monoculture do not develop a stratified morphology with a stratum corneum, do not support lytic growth of ChHV5, and are not positive for herpesviral DNA by quantitative PCR (qPCR) (24).

Our work with rafts suggests that ChHV5 production requires a close interplay between tumor FB and maturing KC. Ballooning degeneration and EII were seen only in the epidermis of plugs or only after the rafts had been raised to the air-liquid interface, thereby stimulating maturation of KC (29), pointing to the critical role that this cell type plays in allowing completion of the replicative cycle of ChHV5. Amplification of viral infectivity in the extreme periphery (maturing KC) makes biological sense because this represents the major source of virus transmission (23). The important role of tumor FB is illustrated in part by raft cultures where KC from normal skin were able to support the *de novo* formation of virus replication sites, though only when they had been layered over tumor FB. The obligate requirement of tumor FB that have been documented to be consistently qPCR positive for herpesviral DNA (24) for production of EII in rafts suggests that this cell type plays an important role in virus growth in KC. Exploring how cell signaling between FB and KC influences virus morphogenesis may

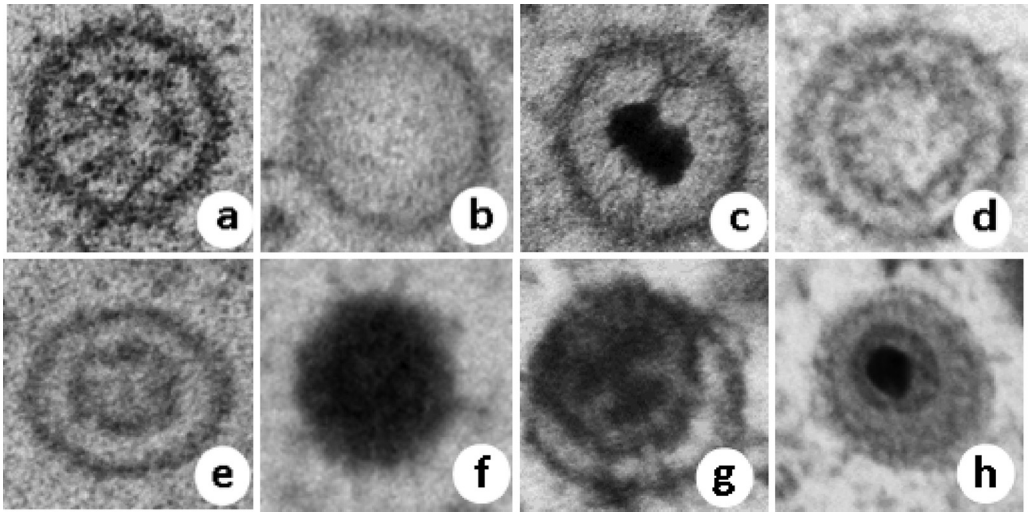

FIG 4 Capsid morphology of ChHV5 seen in the nucleus (a to f) or cytoplasm (f to h) of cultured rafts or plugs. (a) Stippled (plugs only); (b) clear; (c) targetoid; (d) concentric (plugs); (e) concentric (rafts); (f) solid (cytoplasm and nucleus; rafts and plugs); (g) tegumented (plugs); (h) enveloped (plugs). Sizes of capsids are shown in Table 3.

be a promising avenue of research. Perhaps FB represent an important site of latency for ChHV5. Although we failed to detect virus in fibroblasts by electron microscopy, the virus may reactivate at a low abundance before being transferred to KC. This hypothesis fits with the reactivation of latent HSV-1 or HSV-2 as a consequence of cocultivating hardly permissive, latently infected neurons with susceptible and permissive cell lines, such as Vero cells (38, 39).

Interestingly, the use of chemical inducers to grow herpesviruses refractory to *in vitro* cultivation did not appear to positively influence lytic virus growth in rafts or plugs. This also confirms previous attempts to culture ChHV5 in turtle FB or KC where inducers failed to increase viral loads in latently infected monolayers of turtle fibroblasts as tested by qPCR (24). However, we caution that given the low rate of EII production in this study and the variety of inducers tried, it is likely that our ability to detect a statistically significant effect was underpowered. Future studies might benefit from being more strategic in the selection of inducers, focusing on fewer chemicals.

Unique morphological features of ChHV5. For plugs, the most striking findings were highly regular round electron-dense bodies surrounded by viral capsids. Intranuclear amorphous dense bodies associated with various numbers of viral capsids have been seen in monolayer cell cultures infected with pseudorabies virus (PRV) (34), cytomegalovirus (CMV) (37), and HSV-1 (40). While viral proteins were identified in nuclear dense bodies of cells infected with HSV (33) and PRV (34), dense bodies were devoid of nucleic acids (41). Our study is the first to show dense bodies with such a uniform geometry and capsid coverage. The presence of reticulated nuclear bodies with an electron-dense fibrillar network enclosing mainly concentric capsids and partial capsids also does not seem to be documented in the literature; the closest we could find to this is shown in Fig. 3e (showing CMV-infected cells) of reference 42. Similar to the same study, we also observed spherical and polyhedral forms of capsids, which represent different forms of capsid maturation. Finally, we encountered seemingly partial capsids in intranuclear reticular bodies (Fig. 3a), which were remarkably similar to those of late partial HSV-1 capsid assembly in a cell-free system (43). The close association of capsids with these electron-dense bodies, along with evidence of viral proteins in other studies (34, 37), suggests that they are capsid factories. Alternatively, these bodies may be dumping grounds for malformed capsids, but having a virus devote resources to create such large amounts of nonviable particles would seem to make little evolutionary sense from a replication efficiency standpoint.

The variety of capsids seen in plugs was also unusual. Clear, concentric, and targetoid capsids were similar to type A, B, and C capsids described for HSV (44);

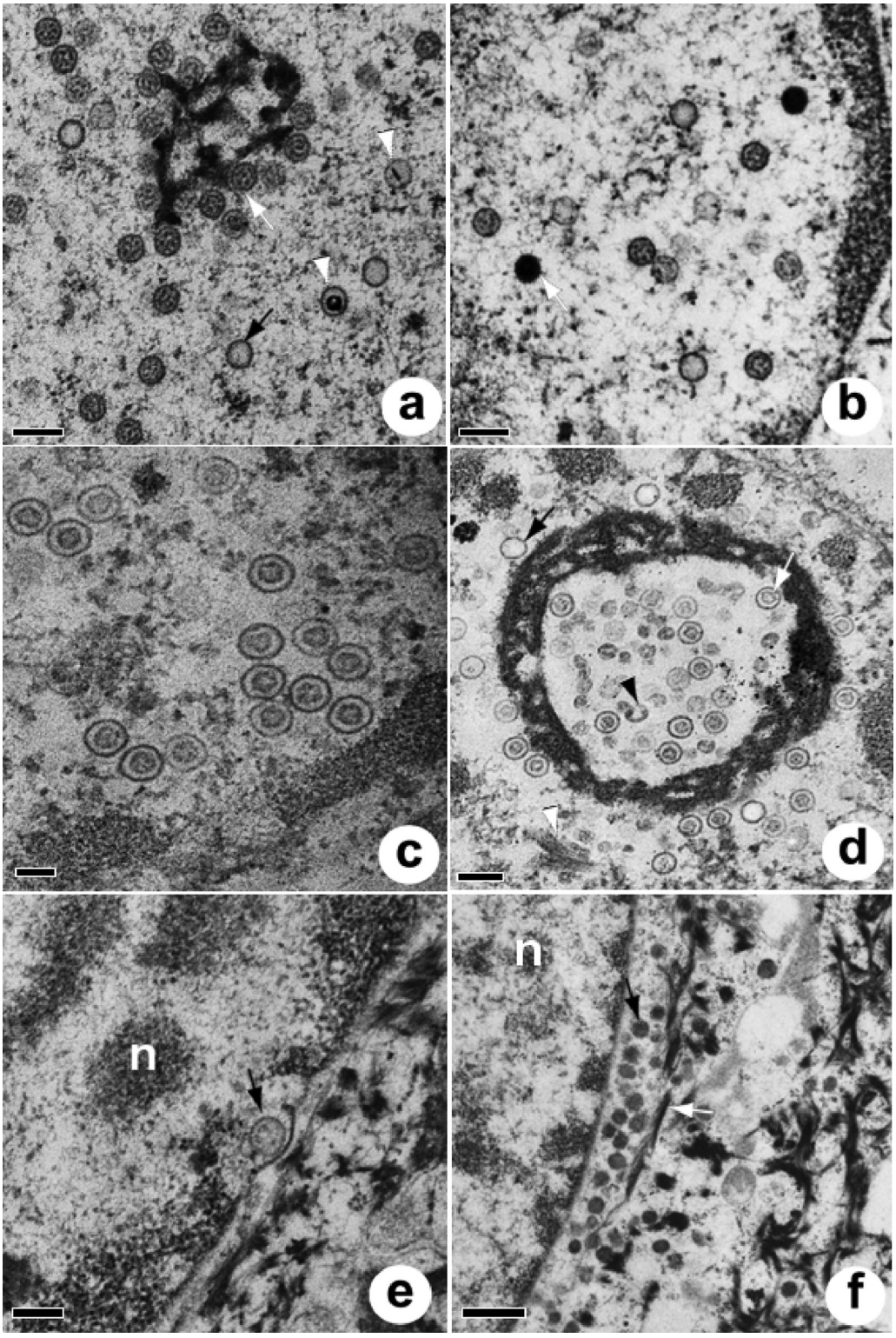

FIG 5 Electron micrographs of plug nuclei (a and b), nuclei of rafts (c and d), and the nuclear-cytoplasmic transition of plugs (e and f). (a) Reticulated intranuclear body with stippled (white arrow), clear (black arrow), and targetoid (white arrowheads) capsids. Bar = 200 nm. (b) Detail of the nucleus showing clear, stippled, and solid (white arrow) capsids. Bar = 200 nm. (c) Nucleus of raft culture, with close-up view of commonly encountered intranuclear concentric capsids. Bar = 100 nm. (d) Reticulated intranuclear body within raft culture, associated with clear (black arrow), concentric (white arrow), and incomplete (black arrowhead) capsids along with tubular crystalline material (white arrowhead). Bar = 200 nm. (e) Budding of viral particle (arrow). Note the dense intrusion of the inner nuclear membrane going into the perinuclear space. Bar = 200 nm. n, nucleus. (f) Perinuclear accumulation of dense capsids filled with DNA (black arrow) closely associated with keratin filaments (white arrow) and adjacent to the fragmented nuclear membrane. Bar = 500 nm. n, nucleus.

TABLE 3 Types, means, SDs, and ranges of diameter of viral capsids within the nucleus and cytoplasm in cultured plugs and rafts[a]

Capsid location and type	Plugs		Rafts	
	Mean ± SD (*n*)	Range of diam (nm)	Mean ± SD (*n*)	Range of diam (nm)
Nucleus				
Clear	100 ± 7 (61)	86–118	111 ± 8 (51)	89–128
Concentric	101 ± 8 (63)	86–124	109 ± 9 (102)	87–131
Stippled	100 ± 6 (60)	86–117	0	0
Targetoid	100 ± 7 (18)	88–111	130 ± 20 (11)	101–177
Solid	101 ± 3 (4)	98–103	94 ± 9 (14)	78–105
Cytoplasm				
Tegumented	214 ± 20 (24)	175–270	TLC	TLC
Nontegumented	217 ± 32 (64)	165–306	TLC	TLC
Enveloped	238 ± 41 (11)	190–306	TLC	TLC

[a]TLC, capsids were too few to count or summed to ≤3. Eight, 19, and 11 cells were enumerated for plug cytoplasm, plug nuclei, and raft nuclei, respectively.

however, we most often saw capsids with stippled scaffolds, most similar to those described for CMV (42) or varicella-zoster virus (45), and electron-dense capsids filled with DNA. For Marek's disease virus (MDV), type A (clear) capsids are most common, with type B (concentric) capsids considered abortive and type C capsids considered mature (46); however, clear criteria for justifying why type B capsids are abortive are lacking. For CMV (47) and PRV (48), type B is the most common type and is considered an intermediate form between types A and C. In contrast, stippled capsids were most common in ChHV5-infected plugs, with types A and C forming a minority. The close association of stippled and concentric capsids with dense bodies (capsid factories) suggests that they are immature, perhaps transitioning from the second most numerous, clear capsids to targetoid and then solid forms. Answering this definitively will require more controlled observations of plugs over time, which is not feasible at present given the low (10%) success rate of viral replication we can currently achieve.

Intranuclear tubular structures associated with partial capsid formation were similar to those observed for lymphocytes infected with human herpesvirus 6 (49), HSV-2-infected Vero cells (50), MDV-infected lymphocytes (51), CMV-infected FB, and other virus-infected cells (for at least 8 other herpesviruses) (52). These tubules have been proposed, though without supportive data, to represent abortive capsids that somehow happen to differentiate into tubular structures due to mistakes in capsid assembly (51, 52). While this may have its logic in the context of infections at exorbitantly high multiplicities of infection (MOI), it would seem maladaptive for viruses in the context of natural replication at low MOI to commit host cell resources to construct such large abortive structures. An equally plausible, though somewhat provocative, explanation may be that these tubular structures represent an early form of capsid production where capsids are assembled via tubular intermediates. Until data on the morphogenesis of these tubules along with identification of viral proteins are provided, their role in herpesviral replication remains an unexplained but potentially important mechanism of viral capsid assembly. Such investigations for ChHV5 await the development of reagents that will allow us to tag viral proteins for electron microscopy.

Intermediate filaments play an important role in development of ChHV5. There was a clear association of naked and tegumented intracytoplasmic capsids with keratin filaments in plugs, and the reasons for this remain unknown. Intermediate filaments, in which keratins are a component, are synthesized from the cell periphery to the center and play an important role in herpesvirus infection, facilitating transport of virus across cell membranes (53). Keratins may also inhibit migration of inflammatory cells to the epidermis, thus shielding viruses from the host immune response (54). Supporting this conjecture is the pathology of epidermal fibropapillomas in green turtles, in which dermal lymphoid infiltrates are common but epidermal inflammation is rare (55). Thus,

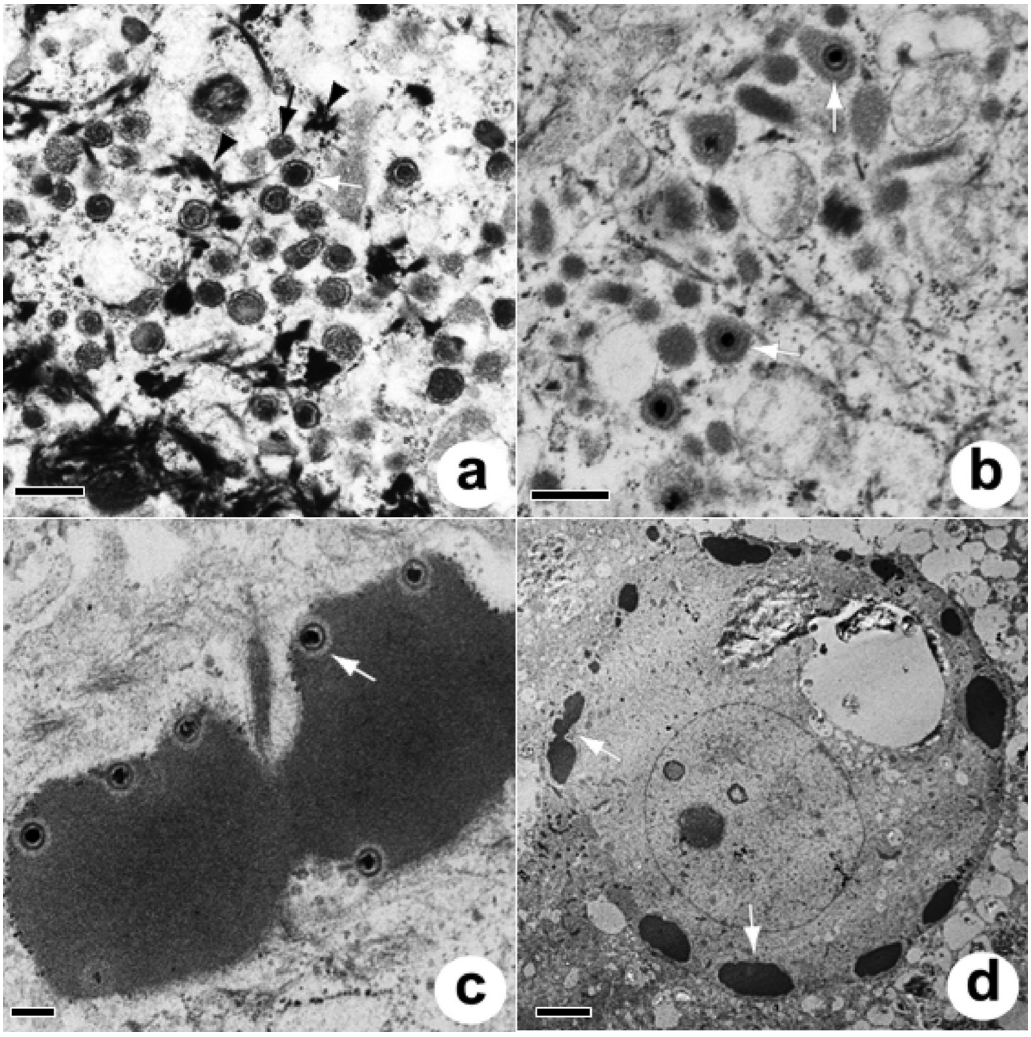

FIG 6 Cytoplasm of plugs. (a) Tegumented (white arrow) and nontegumented (black arrow) capsids associated with keratin filaments (arrowheads) within the cytoplasm of plugs. Bar = 500 nm. (b) Enveloped single capsids (arrows) among delicate fibrils and electron-dense globules within the cytoplasm of plugs. Bar = 400 nm. (c) Multiple capsids enveloped in electron-dense material within the cell cytoplasm (arrow). Bar = 200 nm. (d) Low-magnification view of an infected cell with a swollen nucleus and vacuolated cytoplasm. Note the electron-dense material arrayed near the cell membrane (arrows). Bar = 4 μm.

maturing KC may offer the only refugia where the virus can carry out the entire lytic phase of reproduction and may protect the virus when skin cells are shed, thereby facilitating transmission. Similarities exist for other herpesviruses, such as Epstein-Barr virus (EBV), which remain latent in lymphocytes but are shed in the mucosal epithelium (56).

In contrast to other members of the *Herpesviridae*, for which tegument formation and envelopment are associated with the Golgi complex (57), tegumented particles of ChHV5 appeared to be more closely associated with keratin filaments, whereas enveloped particles occurred in electron-dense material in the cytoplasm, often involving multiple capsids. Capsids in electron-dense material have been seen for MDV (58), ranid herpesvirus 1 (59), and CMV; in the latter case, the dense material contains virus tegument proteins (60). For ChHV5, this electron-dense material containing capsids segregated to cell surfaces, suggesting a tropism for cell membranes or junctions, thereby providing a potential mechanism of cell-cell movement of virus. A parallel exists for HSV-1, as the mature virus has a tropism for desmosomes and tight and adherens junctions (61).

The need to examine herpesviral development in a 3D matrix. Organotypic cultures have been used to look at development of HSV (62), human CMV (HCMV) (63), and EBV (56), but none have been used to examine virus morphogenesis at the ultrastructural level. Indeed, most studies of herpesvirus morphogenesis that focus on electron microscopy have looked at viral growth in monolayer cell cultures. Virus morphogenesis varies depending on the cell culture system (64). Moreover, in many instances, virus isolates were first adapted for optimal growth in cell cultures before electron microscopy studies were carried out. Given this situation, it is highly doubtful that what is seen in monolayers with cell culture-adapted virus strains is completely reflective of what happens in the more complex three-dimensional environment of host tissues with wild-type virus. This point is illustrated by comparing ChHV5 morphogenesis in cultured plug biopsy specimens from tumors, which most closely replicate the host environment, to that in rafts where KC were seeded on a rat tail collagen matrix containing turtle FB. Keratinocytes from plugs had 5 morphologies of intranuclear capsids (clear, concentric, targetoid, solid, and stippled), with the stippled morphology dominating, the presence of nuclear round bodies surrounded with capsids, and numerous intracytoplasmic capsids associated with keratin filaments. Contrast this with raft KC, where concentric capsids dominated in the nucleus, stippled capsids and intranuclear round bodies were absent, and intracytoplasmic capsids were infrequent. Given that plugs are easier to culture than rafts and yield a richer picture of virus morphogenesis, future studies might focus on optimizing plug cultures.

While the raft and plug culture techniques are promising ways to grow ChHV5 *in vitro*, we acknowledge several limitations. Screening for EII in tumors relied on light microscopy examination of a single 5-μm-thick slice of tissue from each tumor. Given the rarity of EII in tumors (23), it is highly likely that we missed many tumors with EII. In contrast, given their small size (3 to 6 mm), lesions in plugs occupied a comparatively larger proportion of the tissue than that in tumors, thereby facilitating more detailed observations of virus growth. Finally, our inability to culture turtle KC through numerous passages and the lack of access to persistently infected FB cell lines required a constant source of tumors and cells, which for a threatened species, such as green turtles, may limit the widespread applicability of using rafts or plugs to grow virus. There are existing techniques to immortalize cells, such as manipulating telomerase (65) or use of stem cells, and these might be future leads to follow. For instance, avian KC stem cells were successfully used to grow MDV (66), and similar techniques might be applicable to turtles.

We think it improbable that our findings are part of the normal morphology of turtle cells, because none of the structures seen in rafts or plugs were present in normal skin of turtles. It is also unlikely that the structures seen here were artifacts of viral inducers, because all the electron micrographs shown here were from cultures that received no viral inducers. Our findings thus paint a picture of ChHV5 morphogenesis that adopts features of various herpesviruses and provides potential new insights into herpesviral capsid assembly. Three-dimensional cultures generate a richer variety and morphology of viral structures than those typically seen in monolayers, and host tissues yield more diverse forms than those in rafts, thus confirming the results of studies of monolayers where different cell types yielded different morphologies (64). Future studies of human herpesvirus morphogenesis might benefit from closer scrutiny of virus development in tissues that more closely replicate the three-dimensional structure of the host. Finally, our findings may help in the management of FP in wild turtles. A better understanding of virus morphogenesis coupled with further refinement of this system may lead to ways to grow cell-free ChHV5 in monolayers. This in turn would allow confirmation of the virus as a cause of FP and validation of serological tests to help elucidate the epidemiology and transmission of ChHV5, all of which are critical pieces of information to aid in future management and mitigation of this disease in endangered green turtles.

MATERIALS AND METHODS

Tissue samples originated from green turtles with severe cases of FP that had a poor prognosis and merited euthanasia for humane reasons (5). All procedures in this study were reviewed and approved by the U.S. Geological Survey National Wildlife Health Center's Animal Care and Use Committee (ACUC protocol ST100407B). Turtles originated from the islands of Kauai, Oahu, Maui, and Hawaii between 2007 and 2009. Immediately after euthanasia, skin biopsy sites were extensively scrubbed for 5 min with soap and water, with copious rinsing, to remove epibionts (algae and barnacles). Subsequently, skin was scrubbed with betadine surgical scrub for 5 min, excised with sterile forceps and scalpel, placed in phosphate-buffered saline (PBS) containing 200 U/ml penicillin, 0.2 mg/ml streptomycin sulfate, 10 μg/ml gentamicin sulfate, and 5 μg/ml amphotericin B (Sigma-Aldrich), and maintained at 4°C until processing within 12 h of collection. Skin from normal wild or captive healthy turtles was prepared the same way, except that sampling was done with 6-mm biopsy punches after infusion of 2% lidocaine at the biopsy site. A subset of tumors was measured and their surface area estimated as described previously (23). We used two strategies to grow ChHV5 in turtle KC, namely, incubations of plugs and rafts.

Tissue plugs. Skin collected from necropsy or biopsy specimens was washed twice in sterile PBS, 3- or 6-mm plugs were collected using sterile disposable skin biopsy punches (Acuderm) and trimmed with a sterile scalpel, and 2 to 4 punch specimens per well of a 24-well plate were equilibrated in Leibowitz L-15 medium (67) supplemented with 10% fetal calf serum (FCS; HyClone), 1 mM sodium butyrate (Sigma), 1 mM nonessential amino acids (HyClone), and growth factors (KGM-2 Single Quots; Lonza) (KC medium) at 30°C for 3 to 7 days. Equilibrated tissue plugs were elevated to the air-liquid interface by placement on mesh grids in 6-well plates containing 3 ml of KC medium and were incubated for 4 to 29 days.

Some plugs were treated with the following chemicals known to induce lytic growth of herpesviruses in tissue culture: 0.5 mM ($n = 21$) or 1 mM ($n = 31$) sodium butyrate or 8 nM ($n = 127$) or 16 nM ($n = 54$) phorbol 12-myristate 13-acetate (TPA) for 24 h every 4 days (68), 10 μM 5-azacytidine ($n = 6$) (69) or 50 μM forskolin ($n = 29$) for 4 days (70), 5 mM hexamethylenebisacetamide (HMBA) ($n = 8$) daily (71), 10 ng/ml tumor necrosis factor alpha (TNF-α) ($n = 8$) daily (72), 20 μg/ml iododeoxyuridine (IUDR) ($n = 11$) for 48 h (73), 10 nM dexamethasone ($n = 2$) for 48 h (74), IUDR for 24 h followed by 10 nM dexamethasone ($n = 3$) for 72 h (74), 1 nM epinephrine ($n = 5$) for 24 h (75), and 5 μM trichostatin A ($n = 9$) or 10 mM valproic acid ($n = 4$) for 18 h (76). All chemicals were from Sigma, except for dexamethasone and epinephrine, which were from Phoenix Pharmaceutical and MP Biomedicals, respectively. After air-liquid interface cultivation, tissue plugs were harvested, and half were fixed in 10% neutral buffered formalin for standard histopathology examination and the other half either frozen (−70°C) or saved in electron microscopy fixative (77).

Rafts (organotypic cultures). For rafts, green turtle KC and FB were cultured in KC medium (as described above) and FB medium (Leibovitz L-15 medium, 10% FCS, 1 mM sodium butyrate [Sigma], 1 mM nonessential amino acids [HyClone], 100 U/ml penicillin, 0.1 mg/ml streptomycin sulfate, 5 μg/ml gentamicin sulfate, and 2.5 μg/ml amphotericin B [all from Sigma]), respectively. FB and KC were identified based on morphology and reactivity to vimentin and pancytokeratin (24). Fibroblasts from tumors were initiated from primary culture or once-frozen stock at passage 3 or less to ensure that cells were virus positive by qPCR (24), whereas FB from normal tissue were initiated from primary culture or once-frozen stock (passages 1 to 43). Collagen gels were made of 2 parts 5× L-15 medium, 1 part reconstitution buffer (2.2% $NaHCO_3$, 0.05 M NaOH, and 0.2 M HEPES buffer, filter sterilized using a 0.22-μm-pore-size filter), 6.5 parts rat tail collagen type 1 in 0.02 N acetic acid (BD) at concentrations ranging from 2 to 6.1 mg/ml, and 0.5 part cell suspension at concentrations ranging from (1 to 5) $\times 10^5$ to 2 $\times 10^6$ cells/gel. Fibroblasts and collagen were mixed, and 0.5- to 2.5-ml aliquots were added to 12- or 24-well plates and allowed to polymerize at 37°C for 1 h. Gels were then equilibrated in FB medium for 0 to 7 days at 30°C. Keratinocytes were cultured in KC medium, and when they reached 80 to 90% confluence, the cells were harvested, overlaid on rafts at concentrations ranging from 1.5×10^5 to 4.75×10^5 cells/gel, and cultured submerged at 30°C for 1 to 13 days. Afterwards, cultures were mechanically detached by sliding a sterile spatula around the gel and then were incubated for 1 h to 4 days at 30 or 37°C in order for the cultures to shrink and become elastic. Cultures were then raised to the air-liquid interface and incubated for an additional 10 to 30 days. Postculture, rafts were processed as described for plugs.

Immunohistochemistry. For histopathology, rafts or plugs were embedded in paraffin, sectioned at 5 μm, stained with hematoxylin and eosin (H&E), and examined for the presence of characteristic EII indicative of herpesviral infection (23). To confirm that EII were ChHV5, we incubated slides with an anti-ChHV5 polyclonal rat antibody (23). We also confirmed that EII could be recognized as foreign antigens by green turtles, as follows. Skin tumors with EII detected by use of H&E were deparaffinized, rehydrated in ethanol, equilibrated in EnVision Flex wash buffer (Dako), and drained. Antigen was recovered by treatment with proteinase K (Dako) for 5 min, followed by washing. Nonspecific peroxidase was blocked with 3% hydrogen peroxide for 10 min, followed by washing. Tissues were blocked with 5% nonfat milk in borate buffer, pH 8 (MB), containing 0.5 M NaCl (high salt) for 30 min, drained, incubated for 30 min with FP-positive turtle serum diluted 1:50 in high-salt MB, washed, incubated for 30 min with anti-7S IgY monoclonal antibodies (78) at 2 μg/ml in antibody diluent (Dako), washed, incubated for 30 min with ImmPRESS peroxidase universal goat anti-rabbit/mouse antibody (undiluted) (Vector Laboratories), and washed again twice. The reaction was visualized by use of diaminobenzidine (Dako). To ensure the specificity of turtle antibodies to EII, we ran the following controls: FP-negative serum against tissues with EII and FP-positive serum against normal skin. To ensure the specificity of reactivity of anti-7S

MAbs, we also ran FP-positive serum against turtle skin with EII but used a MAb against *Campylobacter* instead of anti-7S MAbs. Negative controls for VP26 were run as described previously (23).

Electron microscopy. For electron microscopy, tissues were rinsed in 0.1 M sodium cacodylate buffer containing 0.35 M sucrose and postfixed with 1% osmium tetroxide in 0.1 M sodium cacodylate buffer. Tissue was dehydrated in a graded ethanol series, the ethanol was replaced with propylene oxide, and the tissue was embedded in LX112 epoxy resin. Epoxy-embedded tissues were cut into 1-μm-thick sections and stained with Richardson's stain for light microscopy. For electron microscopy, ultrathin (60 to 80 nm) sections were obtained on an RMC Powertome ultramicrotome, double stained with uranyl acetate and lead citrate, viewed on a Hitachi HT7700 transmission electron microscope (TEM) at 100 kV, and photographed with an AMT XR-41B 2k-by-2k charge-coupled device (CCD) camera. We enumerated the morphological types of capsids in the nucleus and the cytoplasm. All virus-associated structures were measured using ImageJ (79). Electron microscopy of normal turtle skin served as a morphological control.

Statistics. To assess how culture conditions or tumor size influenced the presence/absence of EII, we used Firth's logistic regression (80) with the R package logistf (81). This form of logistic regression uses a penalized maximum likelihood method to account for complete or quasi-separation of the outcome variable (presence/absence of EII) for data sets with low (<20%) percentages of 1 or 0 outcomes. To assess whether cultured plugs with EII were more or less likely to originate from tumors with EII as assessed by histology, we used chi-square analysis. Sizes of viral capsids were compared by standard analysis of variance. All statistical analyses were done with R (82), with an alpha value of 0.05.

ACKNOWLEDGMENTS

The use of trade, product, or firm names is for descriptive purposes only and does not imply endorsement by the U.S. government.

This research was funded by the U.S. Geological Survey. M.A.'s contribution to this research was supported by the Wyss Charitable Endowment.

Brian Stacy kindly critiqued early versions of the manuscript.

REFERENCES

1. Pritchard PCH. 1996. Evolution, phylogeny, and current status, p 1–29. *In* Lutz PL, Musick JA (ed), The biology of sea turtles, vol 1. CRC Press, Boca Raton, FL.
2. Donlan CJ, Wingfield DK, Crowder LB, Wilcox C. 2010. Using expert opinion surveys to rank threats to endangered species: a case study with sea turtles. Conserv Biol 24:1586–1595. https://doi.org/10.1111/j.1523-1739.2010.01541.x.
3. Hargrove S, Work T, Brunson S, Foley AM, Balazs G. 2016. Proceedings of the 2015 international summit on fibropapillomatosis: global status, trends, and population impacts, p 1–85. U.S. Department of Commerce, Washington, DC.
4. Herbst LH. 1994. Fibropapillomatosis of marine turtles. Annu Rev Fish Dis 4:389–425. https://doi.org/10.1016/0959-8030(94)90037-X.
5. Work TM, Balazs GH, Rameyer RA, Morris R. 2004. Retrospective pathology survey of green turtles (*Chelonia mydas*) with fibropapillomatosis from the Hawaiian Islands, 1993–2003. Dis Aquat Org 62:163–176. https://doi.org/10.3354/dao062163.
6. Jones K, Ariel E, Burgess G, Read M. 2016. A review of fibropapillomatosis in green turtles (*Chelonia mydas*). Vet J 212:48–57. https://doi.org/10.1016/j.tvjl.2015.10.041.
7. Work TM, Balazs GH, Wolcott M, Morris RM. 2003. Bacteraemia in Hawaiian green turtles, Chelonia mydas, with fibropapillomatosis. Dis Aquat Org 53:41–46. https://doi.org/10.3354/dao053041.
8. Work TM, Rameyer RA, Balazs GH, Cray C, Chang SP. 2001. Immune status of free-ranging green turtles with fibropapillomatosis from Hawaii. J Wildl Dis 37:574–581. https://doi.org/10.7589/0090-3558-37.3.574.
9. Chaloupka M, Balazs GH, Work TM. 2009. Rise and fall over 26 years of a marine epizootic in Hawaiian green sea turtles. J Wildl Dis 45:1138–1142. https://doi.org/10.7589/0090-3558-45.4.1138.
10. Foley AM, Schroeder BA, Redlow AE, Fick-Child KJ, Teas WG. 2005. Fibropapillomatosis in stranded green turtles (*Chelonia mydas*) from the eastern United States (1980–98): trends and associations with environmental factors. J Wildl Dis 41:29–41. https://doi.org/10.7589/0090-3558-41.1.29.
11. Baptistotte C, Scalfoni JT, Gallo BMG, dos Santos AS, de Castilhos JC, Lima EHSM, Bellini C, Barata PCR. 2001. Prevalence of sea turtle fibropapillomatosis in Brazil, p 111–113. *In* Coyne MS, Clark RD (ed), Proceedings of the Twenty-First Annual Symposium on Sea Turtle Biology and Conservation. NOAA, Philadelphia, PA.
12. Herbst LH, Jacobson ER, Moretti R, Brown T, Sundberg JP, Klein PA. 1995. Experimental transmission of green turtle fibropapillomatosis using cell-free tumor extracts. Dis Aquat Org 22:1–12. https://doi.org/10.3354/dao022001.
13. Jacobson ER, Mansell JL, Sundberg JP, Hajjar L, Reichmann ME, Ehrhart LM, Walsh M, Murru F. 1989. Cutaneous fibropapillomas of green turtles (Chelonia mydas). J Comp Pathol 101:39–52. https://doi.org/10.1016/0021-9975(89)90075-3.
14. Dailey MD, Morris R. 1995. Relationship of parasites (Trematoda: Spirorchidae) and their eggs to the occurrence of fibropapillomas in the green turtle (*Chelonia mydas*). Can J Fish Aquat Sci 52:84–89.
15. Landsberg JH, Balazs GH, Steindinger KA, Baden DG, Work TM, Russel DJ. 1999. The potential role of natural tumour promoters in marine turtle fibropapillomatosis. J Aquat Anim Health 11:199–210. https://doi.org/10.1577/1548-8667(1999)011<0199:TPRONT>2.0.CO;2.
16. Aguirre AA, Balazs GH, Zimmerman B, Galey FD. 1994. Organic contaminants and trace metals in the tissues of Hawaiian green turtles (*Chelonia mydas*) afflicted with fibropapillomas in the Hawaiian islands. Mar Poll Bull 28:109–114. https://doi.org/10.1016/0025-326X(94)90547-9.
17. Santos RG, Martins AS, Torezani E, Baptistotte C, Farias JN, Horta PA, Work TM, Balazs GH. 2010. Relationship between fibropapillomatosis and environmental quality: a case study with *Chelonia mydas* off Brazil. Dis Aquat Org 89:87–95. https://doi.org/10.3354/dao02178.
18. Jacobson ER, Buergelt C, Williams B, Harris RK. 1991. Herpesvirus in cutaneous fibropapillomas of the green turtle *Chelonia mydas*. Dis Aquat Org 12:1–6. https://doi.org/10.3354/dao012001.
19. Quackenbush SL, Work TM, Balazs GH, Casey RN, Rovnak J, Chaves A, DuToit L, Baines JD, Parrish CR, Bowser PR, Casey JW. 1998. Three closely related herpesviruses are associated with fibropapillomatosis in marine turtles. Virology 246:392–399. https://doi.org/10.1006/viro.1998.9207.
20. Lackovich JK, Brown DR, Homer BL, Garber RL, Mader DR, Moretti RH, Patterson AD, Herbst LH, Oros J, Jacobson ER, Curry SS, Klein PA. 1999. Association of herpesvirus with fibropapillomatosis of the green turtle *Chelonia mydas* and the loggerhead turtle *Caretta caretta* in Florida. Dis Aquat Org 37:89–97. https://doi.org/10.3354/dao037089.
21. Rodenbusch CR, Almeida LL, Marks FS, Ataíde MW, Alievi MM, Tavares M, Pereira RA, Canal CW. 2012. Detection and characterization of fibropapilloma associated herpesvirus of marine turtles in Rio Grande do Sul, Brazil. Pesqui Vet Brasil 32:1179–1183. https://doi.org/10.1590/S0100-736X2012001100018.
22. Adams MJ, Carstens EB. 2012. Ratification vote on taxonomic proposals to the International Committee on Taxonomy of Viruses (2012). Arch Virol 157:1411–1422. https://doi.org/10.1007/s00705-012-1299-6.

23. Work TM, Dagenais J, Balazs GH, Schettle N, Ackermann M. 2015. Dynamics of virus shedding and in situ confirmation of chelonid herpesvirus 5 in Hawaiian green turtles with fibropapillomatosis. Vet Pathol 52:1195–1220. https://doi.org/10.1177/0300985814560236.
24. Work TM, Dagenais J, Balazs GH, Schumacher J, Lewis TD, Leong JC, Casey RN, Casey JW. 2009. In vitro biology of fibropapilloma-associated turtle herpesvirus and host cells in Hawaiian green turtles (*Chelonia mydas*). J Gen Virol 90:1943–1950. https://doi.org/10.1099/vir.0.011650-0.
25. Renne R, Zhong W, Herdier B, McGrath M, Abbey N, Kedes D, Ganem D. 1996. Lytic growth of Kaposi's sarcoma-associated herpesvirus (human herpesvirus 8) in culture. Nat Med 2:342–346. https://doi.org/10.1038/nm0396-342.
26. Taylor T, Brockman M, McNamee E, Knipe D. 2002. Herpes simplex virus. Front Biosci 7:d752–d764.
27. Meyers C. 1996. Organotypic (raft) epithelial tissue culture system for the differentiation-dependent replication of papillomavirus. Methods Cell Sci 18:201–210. https://doi.org/10.1007/BF00132885.
28. Fuchs E. 2008. Skin stem cells: rising to the surface. J Cell Biol 180:273–284. https://doi.org/10.1083/jcb.200708185.
29. Green H, Kehinde O, Thomas J. 1979. Growth of cultured human epidermal cells into multiple epithelia suitable for grafting. Proc Natl Acad Sci U S A 76:5665–5668.
30. Pu Y, Bernstein YA, Bernstam LI, Bronaugh RL. 1995. Growing a stratified, cornified primary culture of rat keratinocytes with epidermis-like water permeation barrier. In Vitro Cell Dev Biol Anim 31:283–287. https://doi.org/10.1007/BF02634002.
31. Serra M, Brazis P, Puigdemont A, Fondevila DRV, Torre C, Ferrer L. 2007. Development and characterization of a canine skin equivalent. Exp Dermatol 16:135–142. https://doi.org/10.1111/j.1600-0625.2006.00525.x.
32. Cerrato S, Ramio-Lluch L, Brazis P, Rabanal RM, Fondevila D, Puigdemont A. 2014. Development and characterization of an equine skin-equivalent model. Vet Dermatol 25:475-e–477-e. https://doi.org/10.1111/vde.12134.
33. Baines JD, Jacob RJ, Simmerman L, Roizman B. 1995. The herpes simplex virus 1 UL11 proteins are associated with cytoplasmic and nuclear membranes and with nuclear bodies of infected cells. J Virol 69:825–833.
34. Kopp M, Granzow H, Fuchs W, Klupp B, Mettenleiter TC. 2004. Simultaneous deletion of pseudorabies virus tegument protein UL11 and glycoprotein M severely impairs secondary envelopment. J Virol 78:3024–3034. https://doi.org/10.1128/JVI.78.6.3024-3034.2004.
35. Mettenleiter TC. 2004. Budding events in herpesvirus morphogenesis. Virus Res 106:167–180. https://doi.org/10.1016/j.virusres.2004.08.013.
36. Novoa RR, Calderita G, Arranz R, Fontana J, Granzow H, Risco C. 2006. Virus factories: associations of cell organelles for viral replication and morphogenesis. Biol Cell 97:147–172. https://doi.org/10.1042/BC20040058.
37. Peng L, Ryazantsev S, Sun R, Zhou ZH. 2010. Three-dimensional visualization of gammaherpesvirus life cycle in host cells by electron tomography. Structure 18:47–58. https://doi.org/10.1016/j.str.2009.10.017.
38. Aurelian L, Smith CC. 2000. Herpes simplex virus type 2 growth and latency reactivation by cocultivation are inhibited with antisense oligonucleotides complementary to the translation initiation site of the large subunit of ribonucleotide reductase (RR1). Antisense Nucleic Acid Drug Dev 10:77–85. https://doi.org/10.1089/oli.1.2000.10.77.
39. Stevens JG, Cook ML. 1971. Latent herpes simplex virus in spinal ganglia of mice. Science 173:843–845. https://doi.org/10.1126/science.173.3999.843.
40. Puvion-Dutilleul F, Cebrian J. 1988. Involvement of nucleoli and dense bodies in the intranuclear distribution of some capsid polypeptides in cells infected with herpes simplex virus type 1. J Ultrastruct Mol Struct Res 98:229–242. https://doi.org/10.1016/S0889-1605(88)80916-9.
41. Besse S, Puvion-Dutilleul F. 1996. Intranuclear retention of ribosomal RNAs in response to herpes simplex virus type 1 infection. J Cell Sci 109:119–129.
42. Smith JD, De Harven E. 1973. Herpes simplex virus and human cytomegalovirus replication in WI-38 cells. I. Sequence of viral replication. J Virol 12:919–930.
43. Newcomb WW, Homa FL, Thomsen DR, Booy FP, Trus BL, Steven AC, Spencer JV, Brown JC. 1996. Assembly of the herpes simplex virus capsid: characterization of intermediates observed during cell-free capsid formation. J Mol Biol 263:432–446. https://doi.org/10.1006/jmbi.1996.0587.
44. Rixon FJ. 1993. Structure and assembly of herpesviruses. Semin Virol 4:135–144. https://doi.org/10.1006/smvy.1993.1009.
45. Nii S. 1992. Electron microscopic study on the development of herpesviruses. J Electron Microsc (Tokyo) 41:414–423.
46. Denesvre C. 2013. Marek's disease virus morphogenesis. Avian Dis 57:340–350. https://doi.org/10.1637/10375-091612-Review.1.
47. Tandon R, Mocarski ES, Conway JF. 2015. The A, B, Cs of herpesvirus capsids. Viruses 7:899–914. https://doi.org/10.3390/v7030899.
48. Mettenleiter TC, Saalmuller A, Weiland F. 1993. Pseudorabies virus protein homologous to herpes simplex virus type 1 ICP18.5 is necessary for capsid maturation. J Virol 67:1236–1245.
49. Ohtsuki Y, Daibata M, Bandobashi K, Lee GH, Furihata M, Yokoyama A, Miyoshi I. 2008. Ultrastructural study of the morphogenesis of human herpesvirus 6 type B in human T-lymphotropic virus type I-producing lymphoid cells. Med Mol Morphol 41:204–210. https://doi.org/10.1007/s00795-008-0413-z.
50. Oda H, Mori R. 1976. Electron microscope observations on tubular structures in cells infected with herpes simplex virus type 2. Arch Virol 50:159–168. https://doi.org/10.1007/BF01318010.
51. Campbell JG, Woode GN. 1970. Demonstration of a herpes-type virus in short-term cultured blood lymphocytes associated with Marek's disease. J Med Microbiol 3:463–473. https://doi.org/10.1099/00222615-3-3-463.
52. Akatsuka K, Nii S. 1986. Tubular structures detected in the nuclei of human embryonal lung fibroblasts infected with human cytomegalovirus. Microbiol Immunol 30:289–296. https://doi.org/10.1111/j.1348-0421.1986.tb00945.x.
53. Hertel L. 2011. Herpesviruses and intermediate filaments: close encounters with the third type. Viruses 3:1015–1040. https://doi.org/10.3390/v3071015.
54. Friedman HM. 2006. Keratin, a dual role in herpes simplex virus pathogenesis. J Clin Virol 35:103–105. https://doi.org/10.1016/j.jcv.2005.03.008.
55. Herbst LH, Jacobson ER, Klein PA, Balazs GH, Moretti R, Brown T, Sundberg JP. 1999. Comparative pathology and pathogenesis of spontaneous and experimentally induced fibropapillomas of green turtles (*Chelonia mydas*). Vet Pathol 36:551–564. https://doi.org/10.1354/vp.36-6-551.
56. Temple RM, Zhu J, Budgeon L, Christensen ND, Meyers C, Sample CE. 2014. Efficient replication of Epstein-Barr virus in stratified epithelium in vitro. Proc Natl Acad Sci U S A 111:16544–16549. https://doi.org/10.1073/pnas.1400818111.
57. Mettenleiter TC, Klupp BG, Granzow H. 2009. Herpesvirus assembly: an update. Virus Res 143:222–234. https://doi.org/10.1016/j.virusres.2009.03.018.
58. Couteaudier M, Denesvre C. 2014. Marek's disease virus and skin interactions. Vet Res 45:36. https://doi.org/10.1186/1297-9716-45-36.
59. Stackpole CW. 1969. Herpes-type virus of the frog renal adenocarcinoma. I. Virus development in tumor transplants maintained at low temperature. J Virol 4:75–93.
60. Gibson W, Bogner E. 2013. Morphogenesis of the cytomegalovirus virion and subviral particles, p 230–246. *In* Reddehase MJ, Lemmermann NAW (ed), Cytomegaloviruses: from molecular pathogenesis to intervention, vol 1. Caister Academic Press, Norfolk, United Kingdom.
61. Johnson DC, Webb M, Wisner TW, Brunetti C. 2001. Herpes simplex virus gE/gI sorts nascent virions to epithelial cell junctions, promoting virus spread. J Virol 75:821–833. https://doi.org/10.1128/JVI.75.2.821-833.2001.
62. Hukkanen V, Mikola H, Nykanen M, Syrjanen S. 1999. Herpes simplex virus type 1 infection has two separate modes of spread in three-dimensional keratinocyte culture. J Gen Virol 80:2149–2155. https://doi.org/10.1099/0022-1317-80-8-2149.
63. Hai R, Chu A, Li H, Umamoto S, Rider P, Liu F. 2006. Infection of human cytomegalovirus in cultured human gingival tissue. Virol J 3:84. https://doi.org/10.1186/1743-422X-3-84.
64. Schwartz J, Roizman B. 1969. Similarities and differences in the development of laboratory strains and freshly isolated strains of herpes simplex virus in Hep-2 cells: electron microscopy. J Virol 4:879–889.
65. Lagunoff M, Bechtel J, Venetsanakos E, Roy A, Abbey NW, Herndier BG, McMahon M, Ganem D. 2002. De novo infection and serial transmission of Kaposi's sarcoma-associated herpesvirus in cultured endothelial cells. J Virol 76:2440–2448. https://doi.org/10.1128/jvi.76.5.2440-2448.2002.
66. Couteaudier M, Courvoisier K, Trapp-Fragnet L, Denesvre C, Vautherot JF. 2016. Keratinocytes derived from chicken embryonic stem cells support Marek's disease virus infection: a highly differentiated cell model to study viral replication and morphogenesis. Virol J 13:7. https://doi.org/10.1186/s12985-015-0458-2.
67. Leibovitz L. 1963. The growth and maintenance of tissue-cell cultures in free gas exchange with the atmosphere. Am J Hyg (Lond) 78:173–180.

68. Yu Y, Black J, Goldsmith CS, Browning P, Bhalla K, Offermann M. 1999. Induction of human herpesvirus-8 DNA replication and transcription by butyrate and TPA in BCBL-1 cells. J Gen Virol 80:83–90. https://doi.org/10.1099/0022-1317-80-1-83.
69. Chen J, Ueda K, Sakakibara S, Okuno T, Parravicini C, Corbellino M, Yamashini K. 2001. Activation of latent Kaposi's sarcoma-associated herpesvirus by demethylation of the promoter of the lytic transactivator. Proc Natl Acad Sci U S A 98:4119–4124. https://doi.org/10.1073/pnas.051004198.
70. Smith R, Pizer L, Johnson E, Jr, Wilcox C. 1992. Activation of second-messenger pathways reactivates latent herpes simplex virus in neuronal cultures. Virology 188:311–318. https://doi.org/10.1016/0042-6822(92)90760-M.
71. Bernstein D, Kappes J. 1988. Enhanced in vitro reactivation of latent herpes simplex virus from neural and peripheral tissues with hexamethylenebisacetamide. Arch Virol 99:57–65. https://doi.org/10.1007/BF01311023.
72. Kitano K, Rivas C, Baldwin G, Vera J, Golde D. 1993. Tumor necrosis factor-dependent production of human immunodeficiency virus 1 in chronically infected HL-60 cells. Blood 82:2742–2748.
73. Nazerian K. 1975. Induction of an early antigen of Marek's disease virus in a lymphoblastoid cell line. IARC Sci Publ 11:345–350.
74. Paran M, Gallo R, Richardson L, Wu A. 1973. Adrenal corticosteroids enhance production of type-C virus induced by 5-iodo-2′-deoxyuridine from cultured mouse fibroblasts. Proc Natl Acad Sci U S A 70:2391–2395. https://doi.org/10.1073/pnas.70.8.2391.
75. Chang M, Brown H, Collado-Hidalgo A, Arevalo J, Galic Z, Symensma T, Tanaka L, Hongyu D, Zack J, Sun R, Cole S. 2005. B-adrenoreceptors reactivate Kaposi's sarcoma-associated herpesvirus lytic replication via PKA-dependent control of viral RTA. J Virol 79:13538–13547. https://doi.org/10.1128/JVI.79.21.13538-13547.2005.
76. Countryman JK, Gradoville L, Miller G. 2008. Histone hyperacetylation occurs on promoters of lytic cycle regulatory genes in Epstein-Barr virus-infected cell lines which are refractory to disruption of latency by histone deacetylase inhibitors. J Virol 82:4706–4719. https://doi.org/10.1128/JVI.00116-08.
77. McDowell E, Trump B. 1976. Histological fixatives for diagnostic light and electron microscopy. Arch Pathol Lab Med 100:405–414.
78. Work TM, Dagenais J, Breeden R, Schneemann A, Sung J, Hew B, Balazs GH, Berestecky JM. 2015. Green turtles (*Chelonia mydas*) have novel asymmetrical antibodies. J Immunol 195:5452–5456. https://doi.org/10.4049/jimmunol.1501332.
79. Schneider CA, Rasband WS, Eliceiri KW. 2012. NIH Image to Image J: 25 years of image analysis. Nat Methods 9:671–675. https://doi.org/10.1038/nmeth.2089.
80. Firth D. 1993. Bias reduction of maximum likelihood estimates. Biometrika 80:27–38. https://doi.org/10.1093/biomet/80.1.27.
81. Heinze G, Schemper M. 2002. A solution to the problem of separation in logistic regression. Stat Med 21:2409–2419. https://doi.org/10.1002/sim.1047.
82. Ihaka R, Gentleman R. 1996. R: a language for data analysis and graphics. J Comput Graph Stat 1996:299–314.